STRUCTURAL BIOLOGY COMMUNICATIONS

ISSN 2053-230X

Structure of aspartate β-semialdehyde dehydrogenase from *Francisella tularensis*

N. J. Mank,[a]‡ S. Pote,[a]‡ K.A. Majorek,[b] A. K. Arnette,[a] V. G. Klapper,[a] B. K. Hurlburt[c] and M. Chruszcz[a]*

[a]Department of Chemistry and Biochemistry, University of South Carolina, 631 Sumter Street, Columbia, SC 29208, USA, [b]Department of Molecular Physiology and Biological Physics, University of Virginia, PO Box 800736, Charlottesville, VA 22908, USA, and [c]Agricultural Research Service, Southern Regional Research Center, US Department of Agriculture, 1100 Robert E. Lee Boulevard, New Orleans, LA 70124, USA. *Correspondence e-mail: chruszcz@mailbox.sc.edu

Received 22 September 2017
Accepted 1 December 2017

Edited by P. Dunten, Stanford Synchrotron Radiation Lightsource, USA

‡ These authors made equal contributions to the manuscript.

Keywords: amino-acid biosynthesis; lysine biosynthesis; aspartate β-semialdehyde dehydrogenase; oxidoreductases; *Francisella tularensis*; tularemia.

PDB reference: aspartate β-semialdehyde dehydrogenase, 4woj

Supporting information: this article has supporting information at journals.iucr.org/f

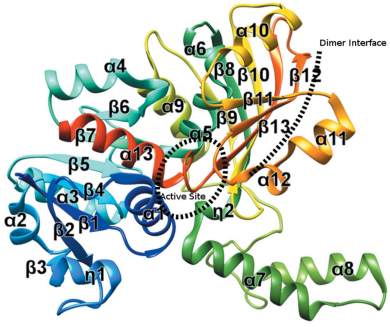

Aspartate β-semialdehyde dehydrogenase (ASADH) is an enzyme involved in the diaminopimelate pathway of lysine biosynthesis. It is essential for the viability of many pathogenic bacteria and therefore has been the subject of considerable research for the generation of novel antibiotic compounds. This manuscript describes the first structure of ASADH from *Francisella tularensis*, the causative agent of tularemia and a potential bioterrorism agent. The structure was determined at 2.45 Å resolution and has a similar biological assembly to other bacterial homologs. ASADH is known to be dimeric in bacteria and have extensive interchain contacts, which are thought to create a half-sites reactivity enzyme. ASADH from higher organisms shows a tetrameric oligomerization, which also has implications for both reactivity and regulation. This work analyzes the apo form of *F. tularensis* ASADH, as well as the binding of the enzyme to its cofactor $NADP^+$.

1. Introduction

Aspartate β-semialdehyde dehydrogenase (ASADH; EC 1.2.1.11) catalyzes the conversion of phosphoaspartate to aspartate β-semialdehyde (L-ASA) *via* reductive dephosphorylation using NADPH as a cofactor (Fig. 1; Karsten & Viola, 1991*a*,*b*). The mechanism is typical of the glyceraldehyde 3-phosphate enzyme family and starts with the formation of a thioester intermediate (Blanco, Moore & Viola, 2003). In the biosynthetic direction for ASADH, a tetrahedral intermediate is formed by nucleophilic attack of the reducing hydrogen, followed by collapse and the expulsion of L-ASA (Hadfield *et al.*, 2001). L-ASA is converted into 4-hydroxy-tetrahydrodipicolinate in the case of diaminopicolinate lysine biosynthesis, or homocysteine in the case of threonine, isoleucine and methionine biosynthesis (Hadfield *et al.*, 1999). ASADH is an essential gene in many bacteria (Akerley *et al.*, 2002; Gerdes *et al.*, 2003; Kobayashi *et al.*, 2003; Sassetti *et al.*, 2003). Mutations that eliminate ASADH activity have been explored as potential vaccine candidates (Cardineau & Curtiss, 1987; Galán *et al.*, 1990; Santander *et al.*, 2010). Lysine and L,L-diaminopimelate are involved in the cross-linking of peptidoglycan monomers in the bacterial cell wall. The essentiality of ASADH and the absence of the lysine-biosynthesis pathway in mammals have also led to extensive research for the development of novel antibiotics (Hutton *et al.*, 2007). Despite these efforts, there are no commercial antibiotics currently available which target ASADH or any part of the diaminopimelate pathway (Sarver *et al.*, 2012).

Francisella tularensis is a Gram-negative pathogenic bacterium that is the causative agent of tularemia. Owing to its

aerosol transmission, low-dose infectivity and high virulence, it is currently listed as a Tier 1 Biological Select Agent by the US Department of Health and Human Services. These attributes also make it a potential agent of biological warfare. As few as 10–50 colony forming units are all that are required to establish infection, and untreated infections can have a fatality rate as high as 30% (Foley & Nieto, 2010). Novel therapeutics against *F. tularensis* are considered to be a high priority for defense against potential bioweapon attacks.

The structure of ASADH from *F. tularensis* (FtASADH) has been determined to a resolution of 2.45 Å. The structure shares many key structural features with known ASADHs from other bacteria, but differs significantly from ASADHs from archaea and fungi. ASADHs from bacteria form functional dimers, while homologs from archaea and fungi form tetramers that may be described as dimers of dimers (Li *et al.*, 2016). This is especially interesting given the intersubunit communication present in the bacterial ASADHs, which leads to a half-sites reactivity model with respect to L-ASA (Nichols *et al.*, 2004). It has also been shown that the tetrameric structure of ASADH from *Trichophyton rubrum* is required for activity, suggesting that the oligomerization state of the ASADH plays a vital role in its activity (Li *et al.*, 2016). This paper will examine the structure of ASADH from *F. tularensis* in the context of classification of enzymes with aspartate β-semialdehyde dehydrogenase activity.

2. Materials and methods

2.1. Protein production and purification

A clone encoding aspartate β-semialdehyde dehydrogenase from *F. tularensis* Schu 4 was obtained from the DNASU plasmid repository (Tempe, Arizona, USA). The gene coding for FtASADH was in the bacterial expression vector pDEST17, which contains an N-terminal hexahistidine tag and is designed for use in an isopropyl β-D-1-thiogalactopyranoside (IPTG) expression system. *Escherichia coli* BL21(DE3) cells were transformed and grown to an OD_{600} of 0.6–0.8, induced with 0.5 m*M* IPTG and grown overnight at 298 K. The bacteria were then centrifuged for 20 min at 10 000*g* and collected. The bacterial cells were resuspended in 50 m*M* Tris, 500 m*M* NaCl, 10 m*M* imidazole pH 8.0 with a protease-inhibitor cocktail (Pierce, Rockford, Illinois, USA), lysed by sonication and the cellular debris was pelleted at 4000*g*. The supernatant was then incubated with Ni–NTA agarose (Qiagen, Chatsworth, California, USA) beads overnight at 277 K with agitation. The beads were then collected, washed with 50 m*M* Tris, 500 m*M* NaCl, 30 m*M* imidazole pH 8.0 and eluted with 50 m*M* Tris, 500 m*M* NaCl, 300 m*M* imidazole pH 8.0. FtASADH was then dialyzed against 10 m*M* Tris, 150 m*M* NaCl, 10 m*M* β-mercaptoethanol overnight at 277 K. The yield of purified FtASADH was approximately 5 mg purified enzyme per litre of culture.

Table 1
Data collection and processing.

Values in parentheses are for the outer shell.

Diffraction source	Beamline 19-BM, APS
Wavelength (Å)	0.9794
Temperature (K)	100
Detector	ADSC Quantum 210r CCD
Space group	*P*1
a, *b*, *c* (Å)	46.59, 60.57, 67.68
α, β, γ (°)	115.43, 100.98, 91.74
Solvent content (%)	40
Mosaicity (°)	0.3
Resolution range (Å)	40.00–2.45 (2.49–2.45)
Total No. of reflections	45447
No. of unique reflections	23498 (1138)
Completeness (%)	97.4 (94.3)
Multiplicity	1.9 (1.8)
$\langle I/\sigma(I)\rangle$	16.9 (3.3)
$R_{\rm r.i.m.}$	0.076 (0.284)
$R_{\rm p.i.m.}$	0.054 (0.201)
Overall *B* factor from Wilson plot (Å^2)	33.2

2.2. Crystallization, data collection and structure determination

The protein concentration was determined by Bradford assay according to the standard protocol (Bio-Rad, Hercules, California, USA). The protein was then concentrated using Microcon centrifugal filters with a nominal molecular-weight limit of 10 kDa (Millipore, Burlington, Massachusetts, USA). Crystallization was performed in 96-well sitting-drop plates (Molecular Dimensions, Altamonte Springs, Florida, USA) by screening with the Index screen (Hampton Research, Aliso Viejo, California, USA). The crystals were formed by mixing 1 µl FtASADH solution (3–5 or 10–15 mg ml^{-1}) with 1 µl well solution and incubating at 298 K. Diffracting, block-shaped crystals with a maximum dimension of approximately 50 µm were obtained from 0.2 *M* ammonium sulfate, 0.1 *M* Tris, 35%(*w*/*v*) PEG 3350 pH 8.5. Single crystals were cryocooled at 100 K and mounted. Data were collected on SBC 19-BM at the Advanced Photon Source, Argonne National Laboratory, Argonne, Illinois, USA (Rosenbaum *et al.*, 2006). Data were processed using *HKL*-2000 (Otwinowski & Minor, 1997). The structure was solved by molecular replacement using *HKL*-3000 (Minor *et al.*, 2006) integrated with *MOLREP* (Vagin & Teplyakov, 2010) and the *CCP*4 software suite (Winn *et al.*, 2011). A single protein chain of the *E. coli* homolog (PDB entry 1t4d; 51% sequence identity; Nichols *et al.*, 2004) was

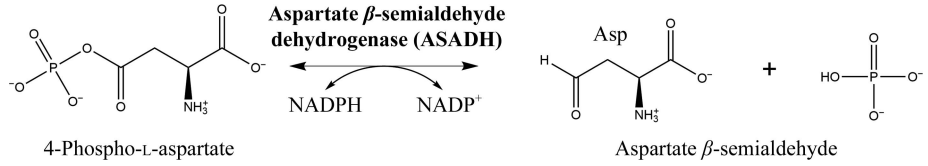

Figure 1
Overview of the reaction catalyzed by ASADH.

Table 2
Structure solution and refinement.

Values in parentheses are for the outer shell.

Resolution range (Å)	37.22–2.45 (2.51–2.45)
Completeness (%)	97.4 (94.5)
σ Cutoff	None
No. of reflections, working set	22134 (1584)
No. of reflections, test set	1180 (89)
Final R_{cryst}	0.183 (0.249)
Final R_{free}	0.238 (0.366)
No. of non-H atoms	
Protein	5653
Ion	16
Water	112
Total	5781
R.m.s. deviations	
Bonds (Å)	0.013
Angles (°)	1.5
Average B factors (Å^2)	
Protein	38.1
Ion	88.6
Water	29.0
Ramachandran plot	
Most favored (%)	95
Allowed (%)	4
Outliers (%)	<1

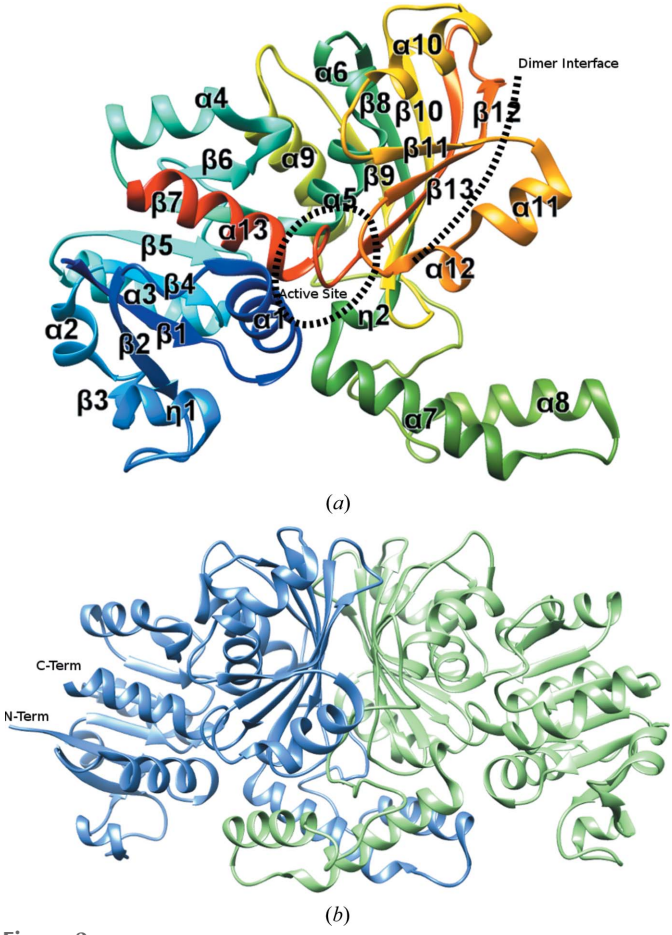

Figure 2
(*a*) The structure of FtASADH is shown with secondary-structure elements labeled. The active site and the dimer interface are marked with dotted lines. (*b*) The dimer assembly of FtASADH is shown with the N- and C-termini labeled. This figure was prepared with *CHIMERA* (Pettersen *et al.*, 2004).

used as a search model. The model obtained after molecular replacement was rebuilt using *Buccaneer* (Cowtan, 2006) and refined using *REFMAC* (Murshudov *et al.*, 2011) and *Coot* (Emsley & Cowtan, 2004). The structure was validated using *MolProbity* (Chen *et al.*, 2010) and *ADIT* (Yang *et al.*, 2004). The final model, together with structure factors, was deposited in the Protein Data Bank (Berman *et al.*, 2000) with accession code 4woj. Summaries of all data-processing and refinement statistics are given in Tables 1 and 2.

2.3. Sequence similarity-based clustering

The full-length sequences corresponding to proteins from Pfam families Semialdhyde_dh (PF01118) and Semialdhyde_dhC (PF02774) were downloaded from the Pfam database (Finn *et al.*, 2016) and merged, followed by the removal of redundant sequences. To visualize sequence similarities between subgroups of related proteins we used *CLANS* (*CLuster ANalysis of Sequences*; Frickey & Lupas, 2004), where the *P*-values of highly scoring segment pairs (HSPs) obtained from an $N \times N$ *BLAST* search are used to compute attractive and repulsive forces between each sequence pair. The clustering was performed using a *P*-value threshold of 1×10^{-3}.

2.4. Isothermal titration calorimetry (ITC)

ASADH enzymatic activity *in vitro* is evaluated using a reaction that proceeds in the nonbiosynthetic direction (Fig. 1) by converting L-ASA into aspartyl-β-phosphate and reducing $NADP^+$ (Black & Wright, 1955; Gao *et al.*, 2010; Holland & Westhead, 1973). Therefore, ITC studies using a VP-ITC MicroCalorimeter (MicroCal, Northampton, Massachusetts, USA) were performed to study the binding of FtASDH to $NADP^+$. Purified enzyme was buffer-exchanged into 25 m*M* HEPES pH 7.5 using gel-filtration chromatography on a Superdex 200 column. The nucleotide solution was prepared in the same buffer. Prior to use, the enzyme and nucleotide solutions were degassed under vacuum using gentle stirring. In all of the experiments the final protein concentration in the sample cell was 55 µ*M*, whereas the ligand concentration was 1.5 m*M*. A 25-injection protocol with 4 µl of ligand per injection spaced at 240 s was used in all of the experiments. The injection syringe was rotated at 310 rev min^{-1} and the temperature was maintained at 298 K. The ligand was also titrated against buffer under the same conditions to obtain heats of dilution for the nucleotide. These data were subtracted from the data with the protein before analysis using the *Origin* software (OriginLab, Northampton, Massachusetts, USA).

3. Results and discussion

3.1. Structure of FtASADH

FtASADH crystallized in space group *P*1 and the structure was determined at 2.45 Å resolution (PDB entry 4woj). Two FtASADH molecules were present in the asymmetric unit. A total of 98% of the residues were modeled, and successive rounds of model building and restrained refinement led to an

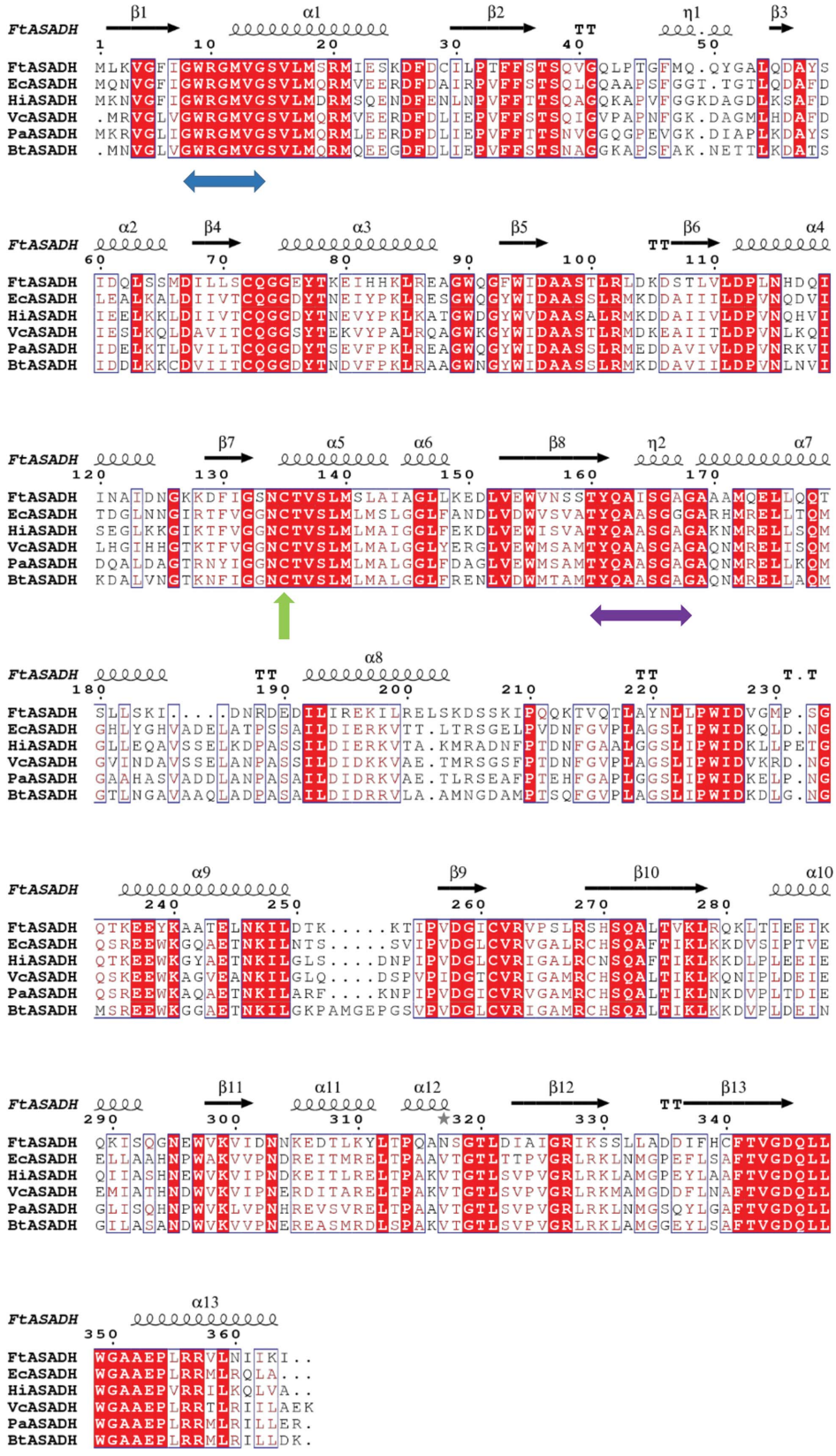

Figure 3
Sequence alignment of ASADHs from *Vibrio cholerae* (VcASADH), *E. coli* (EcASADH), *Pseudomonas aeruginosa* (PaASADH), *Haemophilus influenzae* (HiASADH), *Burkholderia thailandensis* (BhASADH) and *F. tularensis* (FtASADH) that have had their structures determined and belong to the 'aspartate semialdehyde dehydrogenases I' cluster. The catalytic Cys135 is marked with a green arrow. The G*X*X*G*X*X*G motif responsible for nucleoside binding is marked with a blue double-headed arrow. The T*X*QA*X*SG*X*G motif suggested to play a role in active-site communication is marked with purple double-headed arrow. This figure was prepared using *Clustal Omega* (Sievers *et al.*, 2011) and *ESPript* (Robert & Gouet, 2014).

R_{work} of 0.183 and an R_{free} of 0.238. The final model had 95.3% of residues in favored regions, 4.4% in allowed regions and two outliers: Asp227 in chains *A* and *B*. These outliers are in a loop region between α8 and α9. Numbering of the secondary-structure elements is shown in Fig. 2. It is likely that this distortion is owing to a potential salt bridge with Lys240. The structure also contains three bound sulfate ions and a sodium ion. The first sulfate lies on the crystal interface adjacent to Leu114 of chain *A* and forms a hydrogen bond to Asp28 of chain *B* from a symmetry-related element. A second sulfate forms hydrogen bonds to Arg10 of chain *A*. The last sulfate is located between Lys197 and Arg200 of chain *A* and forms hydrogen bonds to Glu23 of chain *B*. The sodium ion is octahedrally coordinated at the crystal interface (Zheng *et al.*, 2014). All of the ions are just artefacts of crystallization and are unlikely to be physiologically relevant. The FtASADH construct contains an N-terminal polyhistidine tag that was completely absent from the density.

FtASADH forms a dimer (Fig. 2*b*) consistent with all known bacterial ASADH structures (Blanco, Moore, Kabaleeswaran *et al.*, 2003; Hadfield *et al.*, 1999; Pavlovsky *et al.*, 2012) and the results of gel filtration (data not shown). The buried area between chains forming the dimer is 3400 Å^2 according to *PDBePISA* (Krissinel & Henrick, 2007). Each chain contains an N-terminal Rossmann NADPH-binding domain and a C-terminal dimerization domain. The N-terminal domain is comprised of four α-helices and seven β-strands, forming a central parallel β-sheet flanked by two α-helical bundles typical of a Rossmann fold. The G*XX*G*XX*G motif responsible for nucleoside binding is present in α1 (Hadfield *et al.*, 1999). The motif is completely conserved in the prokaryotic ASADHs (that have had their structures determined; Fig. 3) starting with residue 8, GMVGSVLM, and differs from the nonprokaryotic sequences only at residues 9, 10 and 12. The G*XX*G*X*VG motif forms the beginning of α1 (Figs. 2*a* and 3). The domain is stabilized by a number of interactions between the side chains of the β-sheet and the α-helices that cradle it. A salt bridge is present between Arg86 in α3 and Asp129 in β7. A second potential salt bridge is present between Arg102 in a loop between β5 and β6 and Glu244 in α9. A series of interdomain salt bridges are formed between Arg20 and Glu353, Arg356 and Asp26, and Arg357 and Asp112. Glu353, Arg356 and Arg357 are all part of α13 of the C-terminal domain, which is inserted between α1 and α4 of the N-terminal domain. This region is likely to be involved in interdomain communication since α1 contains the G*XX*G*XX*G nucleoside-binding motif.

The C-terminal dimerization domain is made up of residues 135–364 and contains secondary-structure elements α5–α13 and β8–β13 (Figs. 2*a* and 3). Helix α13 forms contacts with α1 and α4 of the N-terminal domain, as previously discussed. The central element of the dimerization domain is a six-stranded β-sheet which forms the largest intermolecular interface. α5 is bound in the cleft of the β-sheet and is slightly distorted. The catalytic cysteine, Cys135, is located at the base of α5 (Figs. 3 and 4). A T*X*QA*X*SG*X*G sequence is found in bacterial ASADHSs that have had their structures determined, starting at residue 160, and plays a key role in catalysis and communication between active sites. Residues 169–218 form α7 and α8 and create a distinct arm region that mediates intermolecular contacts outside the central β-sheet.

The central part of the dimerization domain is a six-stranded β-sheet (strands β8–β13) consisting of two pairs of parallel β-strands flanking two central antiparallel strands. The sheets are oriented parallel to the sheet of the second subunit so that many interactions can occur between the side chains of nearby residues. Hydrogen bonds are formed between Thr257 and Asn157, between the two Ser159 residues, and between Tyr161 and the carbonyl O atom of Thr160. A buried hydrophobic patch is also formed by Ile260, Phe341 and Ala273. There are two highly charged regions at opposite ends of the β-sheet. The subunit assembly aligns these highly charged regions in the dimer. These patches are formed by residues 327–336 of a loop in the β-sheet and residues 214–236 of the arm. A series of salt bridges are formed in this region by Arg327, Glu238, Lys329, Asp258 and His339.

3.2. Sequence similarity-based clustering

Clustering classification was carried out to visualize groups of more similar sequences. Clustering was performed based on

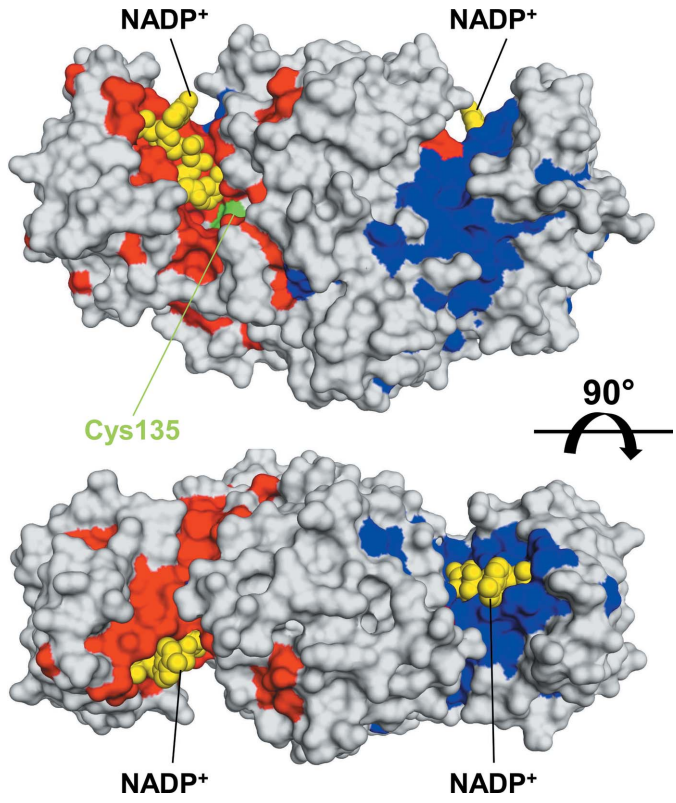

Figure 4
Structure of FtASADH in surface representation. Blue (chain *B*) and red (chain *A*) regions correspond to residues that are conserved in the ASADHs from *V. cholerae*, *E. coli*, *P. aeruginosa*, *H. influenzae*, *B. thailandensis* and *F. tularensis* that have had their structures determined and belong to the 'aspartate semialdehyde dehydrogenases I' cluster. NADP$^+$ (yellow spheres) is modeled using the structure of *H. influenzae* ASADH (PDB entry 1pqu). The active-site Cys135 is shown in green. This figure was prepared with *PyMOL* (DeLano, 2002).

sequence pairwise *BLAST* similarity scores using *CLANS* (Frickey & Lupas, 2004). 4104 full-length sequences of all proteins classified into either of the Pfam domains present in FtASADH [Semialdhyde_dh (PF01118) and Semialdhyde_dhC (PF02774)] were used. The domain organization where both domains are present is the most common architecture among FtASADH homologs. The results are summarized in Fig. 5.

Several groups of sequences could be clearly distinguished, with some sequences scattered in between. Bacterial aspartate semialdehyde dehydrogenases I (ASADH I), which include FtASADH and structurally characterized proteins from *Vibrio cholerae* (PDB entry 3pzr; Pavlovsky *et al.*, 2012), *Pseudomonas aeruginosa* (PDB entry 5bnt; Seattle Structural Genomics Center for Infectious Disease, unpublished work), *E. coli* (PDB entry 1t4b; Nichols *et al.*, 2004) and *Haemophilus influenzae* (HiASADH; PDB entry 1pqu; Blanco *et al.*, 2004), show connections only to a small cluster of *meso*-diaminopimelate D-dehydrogenases and sequences scattered in the central part of the diagram, representing uncharacterized proteins and proteins annotated as nucleoside-diphosphate-sugar epimerases. Similarly, sequences of acetaldehyde dehydrogenases, represented by proteins with known structures, a bifunctional enzyme (aldolase/aldehyde dehydrogenase) from *Thermomonospora curvata* (PDB entry 4lrs; B. Fischer, G. Branlant, F. Talfournier & A. Gruez, unpublished work) and acetaldehyde dehydrogenase from *Mycobacterium tuberculosis* (PDB entry 4jn6; Carere *et al.*, 2013), form a tight cluster connected to the *meso*-diaminopimelate D-dehydrogenases and nucleoside-diphosphate-sugar epimerases. The proteins from the ASADH I group that have had their structures determined have ∼48–51% sequence identity to FtASADH and their structures superimpose with root-mean-square deviations (r.m.s.d.s) in the range 1.0–1.3 Å (over ∼350 C^{α} atoms). Approximately 90% of the sequences in the ASADH I group originate from Gram-negative bacteria.

The largest group of bacterial and plant ASADHs (ASADH II) is represented by aspartate semialdehyde dehydrogenase II from *V. cholerae* (PDB entry 2qz9; Viola *et al.*, 2008) and aspartate semialdehyde dehydrogenases from *Streptococcus pneumoniae* (PDB entry 3q1l; Pavlovsky *et al.*, 2012), *P. aeruginosa* (PDB entry 2hjs; Midwest Center for Structural Genomics, unpublished work), *Thermus thermophilus* (PDB entry 2yv3; RIKEN Structural Genomics/Proteomics Initiative, unpublished work) and *M. tuberculosis* (PDB entry 3tz6; Vyas *et al.*, 2012). Proteins belonging to this group that have had their structures determined have 18–26% sequence identity to FtASADH and their structures superpose with r.m.s.d.s in the range 1.8–2.0 Å (over ∼300 C^{α} atoms). Another large group of ASADHs (ASADH III) is represented by structurally characterized proteins from fungi and archaea: aspartate semialdehyde dehydrogenases from *Candida albicans* (PDB entry 3hsk; Arachea *et al.*, 2010), *Methancoccus jannaschii* (PDB entry 1ys4; Faehnle *et al.*, 2005) and *Sulfolobus tokodaii* (PDB entry 2ep5; RIKEN Structural Genomics/Proteomics Initiative, unpublished work), as well as the paralogous malonyl-CoA reductase from *S. tokodaii* (PDB entry 4dpk; Demmer *et al.*, 2013). It was suggested that the malonyl-CoA reductase from *S. tokodaii* evolved by the duplication of a common ancestral ASADH gene and diverged, gaining a new function (Demmer *et al.*,

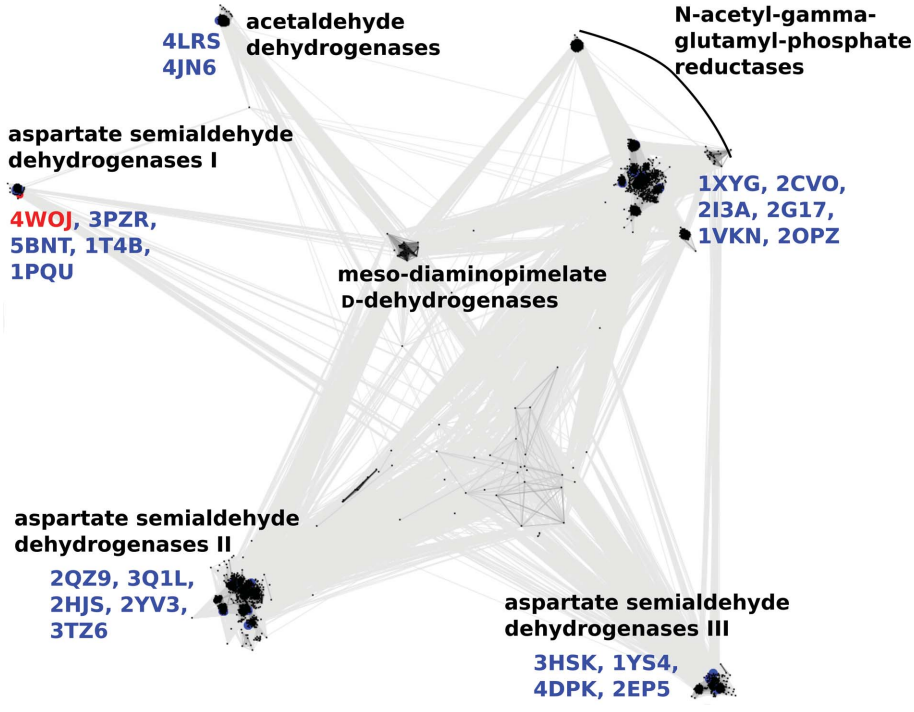

Figure 5
Two-dimensional projection of the *CLANS* clustering results. Proteins are indicated by dots. Lines indicate sequence similarity detectable with *BLAST* and are colored in a spectrum of shades of gray according to the *BLAST P*-value. Sequences corresponding to structures in the PDB are indicated by blue dots.

2013). The members of the ASADH III cluster with determined structures form tetrameric assemblies (Dahal & Viola, 2015, 2017; Li *et al.*, 2016) and have disrupted intersubunit communication that is characteristic of bacterial ASADHs with half-sites enzymatic reactivity (Arachea *et al.*, 2010; Faehnle *et al.*, 2005). Proteins belonging to this group that have had their structures determined have 16–25% sequence identity to FtASADH and their structures superpose with r.m.s.d.s in the range 2.3–2.6 Å (over ∼260 C^{α} atoms).

The largest group with distinguishable subgroups comprises mostly *N*-acetyl-γ-glutamyl-phosphate reductases (ArgCs), including proteins with known structure: ArgCs from *Oryza sativa* (PDB entry 2cvo; Nonaka *et al.*, 2005), *M. tuberculosis* (PDB entry 2i3a; Cherney *et al.*, 2007), *Salmonella typhimurium* (PDB entry 2g17; Midwest Center for Structural Genomics, unpublished work), *Thermotoga maritima* (PDB entry 1vkn; Joint Center for Structural Genomics, unpublished work), *Thermus thermophilus* (PDB entry 2ozp; RIKEN Structural Genomics/Proteomics Initiative, unpublished work) and *Arabidopsis thaliana* (PDB entry 1xyg; Center for Eukaryotic Structural Genomics, unpublished work). Slightly more divergent is a group consisting of some bacterial ArgCs with no structurally characterized representatives.

3.3. Active site of FtASADH and $NADP^+$ binding

The active-site residues are highly conserved amongst all ASADHs (Hadfield *et al.*, 2001). The core is the catalytic cysteine (Figs. 3 and 4), Cys135 in FtASADH, at the base of α5. The sulfur in the active site is not oxidized and there is no disulfide formation despite the inclusion of β-mercaptoethanol in the buffer. There is a single water molecule in the active site which forms a hydrogen bond to Arg263. Arg263 has been implicated in the specificity of the enzyme by forming a salt bridge with the carbonyl of L-ASA (Faehnle *et al.*, 2006). Comparison of the FtASADH apoenzyme with the ternary complex of *E. coli* ASADH (EcASADH; PDB entry 1gl3; Hadfield *et al.*, 2001) shows that the active site undergoes very little movement upon L-ASA binding, and the main movements upon substrate binding occur in the N-terminal domain. The same structure also shows that while both subunits in EcASADH have NADPH bound, L-ASA is bound in only one of the subunits. This half-sites reactivity model is proposed to be owing to communication between subunits by a tetrad consisting of Thr160, Tyr161, Gln162 and Phe345 of EcASADH (Nichols *et al.*, 2004). These residues are conserved in FtASADH and correspond to Thr160, Tyr161, Gln162 and Phe341. This tetrad is located in similar orientations; however, the distance between Phe341 and Tyr161 is longer in EcASADH, which may be owing to the binding of NADPH (Faehnle *et al.*, 2006).

The binding of the cofactor $NADP^+$ to FtASADH was monitored by ITC by titrating the enzyme against $NADP^+$. Fig. 6 (top panel) shows the experimental raw data, in which each peak corresponds to a single injection of $NADP^+$. The dissociation constant (K_d) was determined by fitting the binding isotherm to an equation describing ligand binding to a protein possessing one set of independent sites for the ligand. The integrated titration curve, generated using the *Origin* software, representing the heats of interaction as a function of molar ratio is shown in Fig. 6 (bottom panel). The nonlinear regression analysis of the data yielded a K_d value of 2.9 ± 0.9 μM for $NADP^+$ binding (n = 1.06 ± 0.04 per protein chain, $\Delta H = -8796 \pm 482$ cal mol^{-1}, $\Delta S = -4.2$ cal mol^{-1} K^{-1}, $\Delta G = -7553$ cal mol^{-1}). Previously, a similar K_d of 3.0 ± 0.2 μM was reported for the EcASADH double mutant (Q350N/H171A; Xu *et al.*, 2016). However, wild-type EcASADH bound $NADP^+$ with a K_d of 168 ± 22 μM. On the other hand, a K_d of 6.0 ± 0.8 μM has been reported for ASADH from *S. pneumoniae* (Faehnle *et al.*, 2006). The same manuscript reported K_d values of 17.0 ± 0.3 μM and 10.0 ± 0.2 μM for ASADHs from *H. influenzae* and *V. cholerae*, respectively.

$NADP^+$ binding to ASADH results in a slight closure of the cleft between the N-terminal and C-terminal domains. $NADP^+$ makes extensive backbone hydrogen bonds to Met12, Val13, Thr37 and Ser166 when bound to HiASADH, all of which are conserved in FtASADH. However, the most extensive binding takes place at the 2′-phosphate of $NADP^+$. There is extensive hydrogen bonding to Arg10, Thr37 and Gln74 (Fig. 7). In the apo FtASADH structure, Thr37 and Gln73 are solvent-exposed, while Arg10 is loosely bound to a sulfate ion.

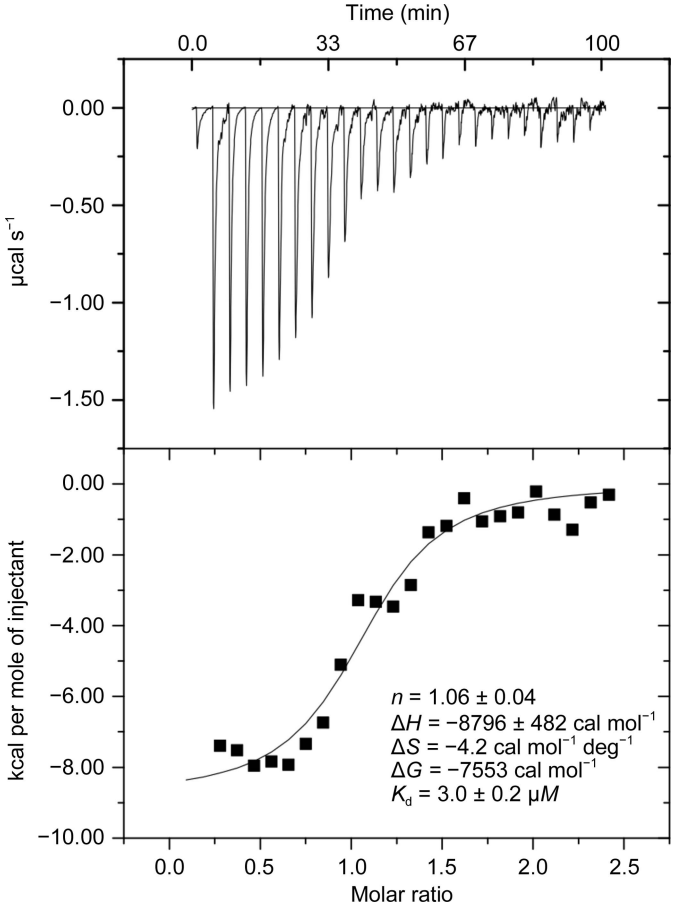

Figure 6
$NADP^+$ binding to FtASADH: ITC. The top panel shows the raw data, while the bottom panel shows the titration curve generated using the *Origin* software.

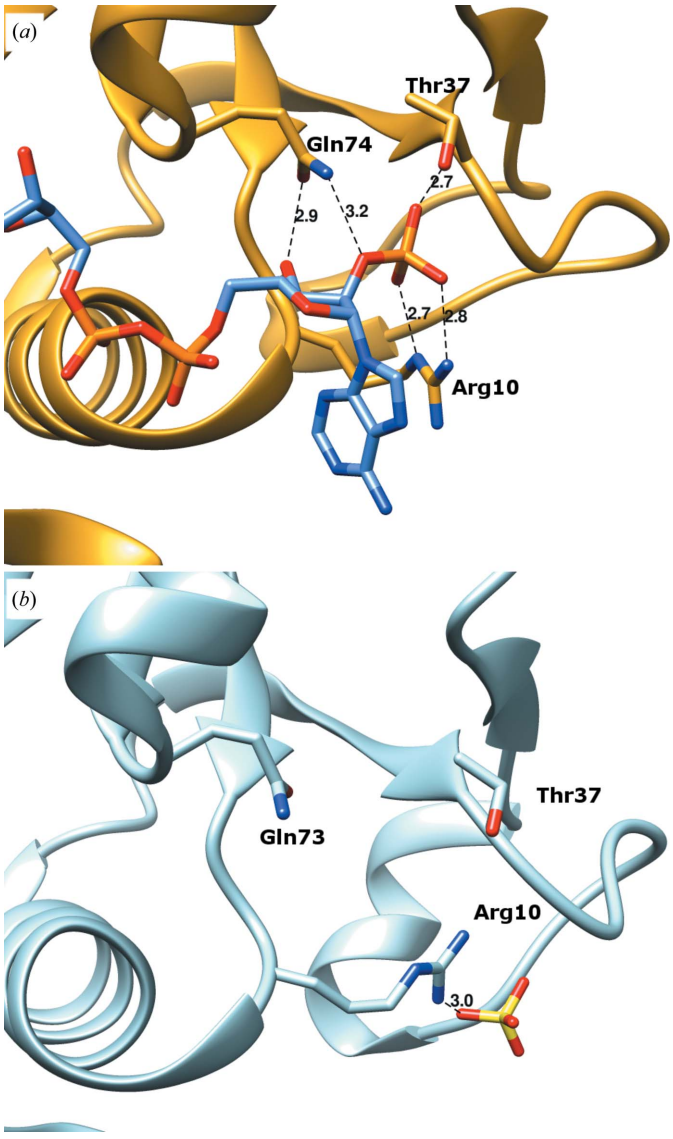

Figure 7
(*a*) The structure of HiASADH with NADP$^+$ (PDB entry 1pqu). The residues responsible for the strong binding of the NADP$^+$ phosphate are shown. (*b*) The structure of apo FtASADH with the corresponding residues. All measurements are given in Å.

4. Conclusion

The structure of the essential enzyme ASADH from the potential bioterrorism agent *F. tularensis* has been determined in the apo form. Sequence and structure analysis allow easy classification of ASADHs. The similarities and differences between enzymes belonging to various groups of ASADHs, which are highlighted in Figs. 4 and 5, suggest the possibility of developing both broad-spectrum as well as selective antibiotics targeting these enzymes.

Acknowledgements

The results shown in this report were derived from work performed at the Structural Biology Center (SBC) at the Advanced Photon Source, Argonne National Laboratory.

Funding information

SBC-CAT is operated by UChicago Argonne LLC for the US Department of Energy, Office of Biological and Environmental Research under contract DE-AC02-06CH11357.

References

Akerley, B. J., Rubin, E. J., Novick, V. L., Amaya, K., Judson, N. & Mekalanos, J. J. (2002). *Proc. Natl Acad. Sci. USA*, **99**, 966–971.
Arachea, B. T., Liu, X., Pavlovsky, A. G. & Viola, R. E. (2010). *Acta Cryst.* D**66**, 205–212.
Berman, H. M., Westbrook, J., Feng, Z., Gilliland, G., Bhat, T. N., Weissig, H., Shindyalov, I. N. & Bourne, P. E. (2000). *Nucleic Acids Res.* **28**, 235–242.
Black, S. & Wright, N. G. (1955). *J. Biol. Chem.* **213**, 39–50.
Blanco, J., Moore, R. A., Faehnle, C. R., Coe, D. M. & Viola, R. E. (2004). *Acta Cryst.* D**60**, 1388–1395.
Blanco, J., Moore, R. A., Kabaleeswaran, V. & Viola, R. E. (2003). *Protein Sci.* **12**, 27–33.
Blanco, J., Moore, R. A. & Viola, R. E. (2003). *Proc. Natl Acad. Sci. USA*, **100**, 12613–12617.
Cardineau, G. A. & Curtiss, R. III (1987). *J. Biol. Chem.* **262**, 3344–3353.
Carere, J., McKenna, S. E., Kimber, M. S. & Seah, S. Y. K. (2013). *Biochemistry*, **52**, 3502–3511.
Chen, V. B., Arendall, W. B., Headd, J. J., Keedy, D. A., Immormino, R. M., Kapral, G. J., Murray, L. W., Richardson, J. S. & Richardson, D. C. (2010). *Acta Cryst.* D**66**, 12–21.
Cherney, L. T., Cherney, M. M., Garen, C. R., Niu, C., Moradian, F. & James, M. N. G. (2007). *J. Mol. Biol.* **367**, 1357–1369.
Cowtan, K. (2006). *Acta Cryst.* D**62**, 1002–1011.
Dahal, G. & Viola, R. E. (2015). *Acta Cryst.* F**71**, 1365–1371.
Dahal, G. P. & Viola, R. E. (2017). *Acta Cryst.* F**73**, 36–44.
DeLano, W. L. (2002). *PyMOL*. http://www.pymol.org.
Demmer, U., Warkentin, E., Srivastava, A., Kockelkorn, D., Pötter, M., Marx, A., Fuchs, G. & Ermler, U. (2013). *J. Biol. Chem.* **288**, 6363–6370.
Emsley, P. & Cowtan, K. (2004). *Acta Cryst.* D**60**, 2126–2132.
Faehnle, C. R., Le Coq, J., Liu, X. & Viola, R. E. (2006). *J. Biol. Chem.* **281**, 31031–31040.
Faehnle, C. R., Ohren, J. F. & Viola, R. E. (2005). *J. Mol. Biol.* **353**, 1055–1068.
Finn, R. D., Coggill, P., Eberhardt, R. Y., Eddy, S. R., Mistry, J., Mitchell, A. L., Potter, S. C., Punta, M., Qureshi, M., Sangrador-Vegas, A., Salazar, G. A., Tate, J. & Bateman, A. (2016). *Nucleic Acids Res.* **44**, D279–D285.
Foley, J. E. & Nieto, N. C. (2010). *Vet. Microbiol.* **140**, 332–338.
Frickey, T. & Lupas, A. (2004). *Bioinformatics*, **20**, 3702–3704.
Galán, J. E., Nakayama, K. & Curtiss, R. III (1990). *Gene*, **94**, 29–35.
Gao, G., Liu, X., Pavlovsky, A. & Viola, R. E. (2010). *J. Biomol. Screen.* **15**, 1042–1050.
Gerdes, S. Y. *et al.* (2003). *J. Bacteriol.* **185**, 5673–5684.
Hadfield, A., Kryger, G., Ouyang, J., Petsko, G. A., Ringe, D. & Viola, R. (1999). *J. Mol. Biol.* **289**, 991–1002.
Hadfield, A., Shammas, C., Kryger, G., Ringe, D., Petsko, G. A., Ouyang, J. & Viola, R. E. (2001). *Biochemistry*, **40**, 14475–14483.
Holland, M. J. & Westhead, E. W. (1973). *Biochemistry*, **12**, 2264–2270.
Hutton, C. A., Perugini, M. A. & Gerrard, J. A. (2007). *Mol. Biosyst.* **3**, 458–465.
Karsten, W. E. & Viola, R. E. (1991*a*). *Arch. Biochem. Biophys.* **287**, 60–67.
Karsten, W. E. & Viola, R. E. (1991*b*). *Biochim. Biophys. Acta*, **1077**, 209–219.
Kobayashi, K. *et al.* (2003). *Proc. Natl Acad. Sci. USA*, **100**, 4678–4683.
Krissinel, E. & Henrick, K. (2007). *J. Mol. Biol.* **372**, 774–797.

Li, Q., Mu, Z., Zhao, R., Dahal, G., Viola, R. E., Liu, T., Jin, Q. & Cui, S. (2016). *Sci. Rep.* **6**, 21067.
Minor, W., Cymborowski, M., Otwinowski, Z. & Chruszcz, M. (2006). *Acta Cryst.* D**62**, 859–866.
Murshudov, G. N., Skubák, P., Lebedev, A. A., Pannu, N. S., Steiner, R. A., Nicholls, R. A., Winn, M. D., Long, F. & Vagin, A. A. (2011). *Acta Cryst.* D**67**, 355–367.
Nichols, C. E., Dhaliwal, B., Lockyer, M., Hawkins, A. R. & Stammers, D. K. (2004). *J. Mol. Biol.* **341**, 797–806.
Nonaka, T., Kita, A., Miura-Ohnuma, J., Katoh, E., Inagaki, N., Yamazaki, T. & Miki, K. (2005). *Proteins*, **61**, 1137–1140.
Otwinowski, Z. & Minor, W. (1997). *Methods Enzymol.* **276**, 307–326.
Pavlovsky, A. G., Liu, X., Faehnle, C. R., Potente, N. & Viola, R. E. (2012). *Chem. Biol. Drug Des.* **79**, 128–136.
Pettersen, E. F., Goddard, T. D., Huang, C. C., Couch, G. S., Greenblatt, D. M., Meng, E. C. & Ferrin, T. E. (2004). *J. Comput. Chem.* **25**, 1605–1612.
Robert, X. & Gouet, P. (2014). *Nucleic Acids Res.* **42**, W320–W324.
Rosenbaum, G. *et al.* (2006). *J. Synchrotron Rad.* **13**, 30–45.
Santander, J., Xin, W., Yang, Z. & Curtiss, R. (2010). *PLoS One*, **5**, e15944.
Sarver, J. G., Trendel, J. A., Bearss, N. R., Wang, L., Luniwal, A., Erhardt, P. W. & Viola, R. E. (2012). *J. Biomol. Screen.* **17**, 673–682.
Sassetti, C. M., Boyd, D. H. & Rubin, E. J. (2003). *Mol. Microbiol.* **48**, 77–84.
Sievers, F., Wilm, A., Dineen, D., Gibson, T. J., Karplus, K., Li, W., Lopez, R., McWilliam, H., Remmert, M., Söding, J., Thompson, J. D. & Higgins, D. G. (2011). *Mol. Syst. Biol.* **7**, 539.
Vagin, A. & Teplyakov, A. (2010). *Acta Cryst.* D**66**, 22–25.
Viola, R. E., Liu, X., Ohren, J. F. & Faehnle, C. R. (2008). *Acta Cryst.* D**64**, 321–330.
Vyas, R., Tewari, R., Weiss, M. S. & Karthikeyan, S. (2012). *Acta Cryst.* D**68**, 671–679.
Winn, M. D. *et al.* (2011). *Acta Cryst.* D**67**, 235–242.
Xu, X., Chen, J., Wang, Q., Duan, C., Li, Y., Wang, R. & Yang, S. (2016). *Chembiochem*, **17**, 56–64.
Yang, H., Guranovic, V., Dutta, S., Feng, Z., Berman, H. M. & Westbrook, J. D. (2004). *Acta Cryst.* D**60**, 1833–1839.
Zheng, H., Chordia, M. D., Cooper, D. R., Chruszcz, M., Müller, P., Sheldrick, G. M. & Minor, W. (2014). *Nature Protoc.* **9**, 156–170.